ELSEVIER

Surface Science 371 (1997) 307–315

surface science

Local structure of Sn/Si(001) surface phases

P.F. Lyman [a], M.J. Bedzyk [a,b,*]

[a] *Department of Materials Science and Engineering and Materials Research Center, Northwestern University, Evanston, IL 60208, USA*
[b] *Materials Science Division, Argonne National Laboratory, Argonne, IL 60439, USA*

Received 7 March 1996; accepted for publication 23 July 1996

Abstract

The surface structures of the (6×2), $c(8\times4)$ and (5×1) phases of Sn/Si(001) were studied using the X-ray standing wave technique. Using the (004) and (022) Bragg reflections, we find that the (6×2) and $c(8\times4)$ phases are composed of highly buckled Sn–Sn ad-dimers located 1.58 Å above the bulk-like Si(004) surface atomic plane. The Sn atoms occupy two distinct sites with a vertical separation of 0.68 Å, resulting in a dimer buckling angle of approximately 14°. Occupation of second-layer sites by Sn in the (5×1) phase, and even in the high-coverage region of the $c(8\times4)$ phase, changes the Sn spatial distribution normal to the surface, which we attribute to unbuckling and/or breaking of the dimers in the first layer.

Keywords: Auger electron spectroscopy; Low-index single crystal surfaces; Photon absorption spectroscopy; Silicon; Surface relaxation and reconstruction; Surface structure, morphology, roughness and topography; Tin; X-ray scattering, diffraction and reflection

1. Introduction

Various motivations have led to previous studies of the adsorption of Sn or Pb on Si and Ge surfaces. Due to negligible solid solubility of these heavy group-IV elements in Si and Ge, the resulting interfaces are thought to be abrupt, and can therefore pose as model systems for Schottky barrier studies [1–3]. Other motivations have sprung indirectly from this lack of solubility; for example, Sn can be used as a (possibly electrically neutral) segregant in surfactant-mediated epitaxy of Si or Ge [4,5]. From a different perspective, this segregation behavior is at unfortunate odds with the creation of metastable SnSi or SnGe alloys [6–9], which are predicted to have exciting electronic properties [10,11]. Finally, one can view adsorption of Sn on Si as a prototype of extremely mismatched epitaxy, characterized by the attendant Stranski–Krastanov growth mode [12].

Throughout the existing studies, little quantitative work has been undertaken to reveal the surface structure of a heavy group IV element on Si(001) or Ge(001). The present work seeks to quantify the coverage-dependent adsorption structure of Sn/Si(001). The rich set of surface superstructures encountered in this system had been uncovered using electron diffraction techniques [13,14], and an attempt to infer the local adsorption sites was made using photoemission spectroscopy [1]. However, essentially no direct atomic-scale information was available until the revealing study of Baski et al. using scanning tunneling microscopy (STM) [15]. This work showed that for a range

* Corresponding author. Northwestern University, Dept. of MS&E, 2225 N. Campus Dr., Evanston, IL 60208, USA. Fax: +1 847 491 7820; e-mail: bedzyk@nwu.edu

Published by Elsevier Science B.V.
PII S0039-6028(96)01007-2

of Sn coverages, the existing surface phases are constructed of subunits having essentially the same local structure, which has been interpreted as a highly buckled dimer. This range extends from about 0.4 to 1.0 monolayer (ML). It was not clear in the STM or other studies whether the dimers are composed of Sn–Sn pairs, Sn–Si pairs or of a mixture [1,15]. Using X-ray standing waves (XSW), we find that Sn/Si(001) surfaces in this coverage range are composed principally of Sn–Sn dimers centered 1.58 Å above the bulk-like Si(004) surface atomic plane. The buckling angle of an ad-dimer at Sn coverages below 0.75 ML is $\sim 14°$; the atomic spatial distribution becomes less broad at Sn coverages above 0.75 ML. We attribute this change to occupation by Sn of second-layer sites.

2. Experimental

The experiments were conducted at beamline X15A of the National Synchrotron Light Source at Brookhaven National Laboratory. The apparatus consists of several coupled ultrahigh vacuum (UHV) chambers (base pressure $\sim 9 \times 10^{-11}$ Torr) allowing sample preparation [molecular beam epitaxial (MBE) growth] and characterization [low energy electron diffraction (LEED), Auger electron spectroscopy (AES) and XSW]. The XSW technique and the experimental arrangement at X15A have been extensively reviewed by Zegenhagen [16].

The Si(001) samples were Syton-polished and chemically cleaned ex situ using the Shiraki process [17], and then mounted in a strain-free manner. After degassing each sample in UHV, the oxide was thermally desorbed at 900°C. Upon cooling to room temperature (initial cooling rate $\approx 2.0°C\ s^{-1}$), a sharp, two-domain (2×1) LEED pattern was observed. AES could detect no O and typically a small amount of C contamination (~ 0.02 ML).

Sn was deposited on the single crystal Si(001) substrates at room temperature (RT) from an effusion cell at ~ 0.5 ML min^{-1} ($1\ ML = 6.78 \times 10^{14}\ cm^{-2}$). Various final Sn coverages were produced by thermal desorption: a slight excess of Sn was first deposited (~ 1.5 ML), then the substrate was heated to temperatures ranging from 570 to 720°C for 10 min to cause Sn desorption and ordering [14]. The background pressure remained $< 3 \times 10^{-10}$ Torr for Sn growth and desorption. This procedure resulted in clear LEED patterns of (with decreasing coverage): facetted (5×1), unfacetted (5×1), $c(8 \times 4)$ and (6×2). All of these superstructures had been previously reported [14], but the $c(4 \times 4)$ reported by Ueda and others to occur at lower coverages was never observed. Coverages were determined by AES and LEED observations as discussed in the next section. Each sample was discarded after Sn desorption resulted in a coverage below the coverage range of interest, and a fresh sample was prepared for the next high-coverage measurement.

For XSW analysis, the incident X-ray beam from the synchrotron radiation source was collimated and monochromated by a double-crystal monochromator and directed through a Be window into the UHV chamber. The sample was held at room temperature and placed so that the X-ray beam was Bragg-reflected by either the (004) or the (022) set of diffraction planes, using 6.2 and 6.8 keV X-rays, respectively. For convenience, we examined XSW scans from only one set of (*hkl*) planes as each new Sn preparation was created on a given sample by thermal desorption; thus, the (004) and (022) data were acquired on different Sn surface preparations. Angular piezoelectric drives on both monochromator crystals were used to precisely scan through the several arc-seconds-wide Bragg reflection. The resultant Sn L fluorescence yield was detected by a energy-dispersive Si(Li) detector, while the reflected X-ray beam was measured by an in vacuo Si photodiode.

3. Coverage calibration (AES)

The coverage ranges corresponding to various LEED superstructures have been reported before as: $c(4 \times 4)$ for 0.2–0.375 ML, (6×2) for 0.375–0.5 ML, $c(8 \times 4)$ for 0.5–1.0 ML, clear (5×1) for 1.0 to 1.5 ML, and facetted (5×1) above 1.5 ML [14]. Coverages in earlier work were derived from AES analysis (compared to bulk signals) and Sn deposition rate on a quartz-crystal oscillator. The calibration of these assignments is therefore somewhat

uncertain. Our AES results and analysis were not sensitive enough [18] to confirm or disprove the coverage assignments for the LEED superstructures. Therefore, we will cite coverages assuming the earlier assignments are accurate. We feel that the absolute coverage assignments remain an open question, but that the previous assignments are most likely correct.

For each surface preparation, we measured the intensity of the Si LVV (92 eV), Si KLL (1619 eV) and Sn MNN (430 eV) transitions. To an excellent approximation, the (Sn MNN)/(Si KLL) AES ratio will be directly proportional to Sn coverage over the range of interest due to the relatively long mean free path of Si KLL electrons. The (Sn MNN)/(Si LVV) ratio should deviate from linearity due to attenuation of the low-energy Si line. Fig. 1 shows a graph of the measured (Sn MNN)/(Si LVV) ratio versus (Sn MNN)/(Si KLL) ratio for a number of sample preparations. This treatment minimized errors associated with the analysis conditions changing from spectrum to spectrum. The solid line in Fig. 1 is a fit to a layer-by-layer growth model derived assuming exponential absorption probabilities. The LEED pattern observed for these samples is indicated schematically. The quality of the fit to the growth model substantiates laminar growth over this coverage range and reflects the low relative uncertainty of the AES measurements. By comparison to the

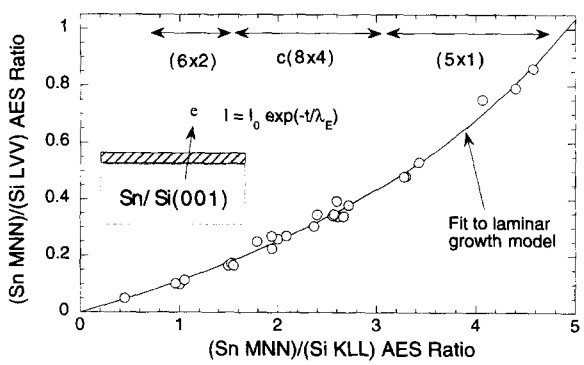

Fig. 1. For various preparations of Sn/Si(001), the measured (Sn MNN)/(Si LVV) Auger ratio versus (Sn MNN)/(Si KLL) Auger ratio. The solid line is a fit to a growth model assuming layer-by-layer growth and exponential absorption probabilities of Auger electrons. The LEED patterns observed are indicated schematically.

growth model and the LEED patterns (using Ueda's assignments [14]), we find that a (Sn MNN)/(Si KLL) AES ratio of 3.10 ± 0.15 corresponds to 1 ML.

4. Local structure (XSW)

The XSW technique is conducted by Bragg-reflecting a monochromatic X-ray beam from a single crystal sample. In the dynamical regime [19], the interference of the coherently coupled incident and reflected plane waves generates an XSW in and above the crystal, with the XSW nodal planes parallel to and having the same periodicity as the diffraction planes. The phase of the standing wave with respect to the diffraction planes shifts by 180° as the Bragg angle θ is scanned from the low-angle side of the rocking curve to the high-angle side. This phase shift moves the antinodal planes of the standing wave inward by one-half of the d-spacing d_{hkl}. Thus, the angular dependence of the normalized fluorescence yield $Y(\theta)$ from an adatom layer can be described as:

$$Y(\theta) = 1 + R(\theta) + 2\sqrt{R(\theta)} f_H \cos[v(\theta) - 2\pi P_H], \quad (1)$$

where $R(\theta)$ is the reflectivity and $v(\theta)$ is the relative phase of the diffracted plane wave. The coherent fraction f_H and coherent position P_H correspond to the amplitude and phase, respectively, of the Hth Fourier component of the time-averaged spatial distribution of the nuclei of the adatoms (projected into a unit cell). $\boldsymbol{H}$ is the reciprocal lattice vector for the (hkl) diffraction planes. More specifically, the coherent fraction can be written as the product of three factors [20]:

$$f_H = C a_H D_H, \quad (2)$$

where C is the fraction of adatoms at ordered positions, a_H is a geometrical factor and D_H is the Debye–Waller factor. The Debye–Waller factor can be expressed as $D_H = \exp(-2\pi^2 \langle u_H^2 \rangle / d_H^2)$, where $\langle u_H^2 \rangle$ is the mean-squared thermal vibrational amplitude of the adatom in the $\boldsymbol{H}$ direction.

Except for certain special coverages, the symmetry and structure of Sn/Si(001) has been shown to be a complicated function of Sn coverage and sample preparation history [15]. Particularly at

lower coverages, a variety of coexisting local periodicities is observed. In general, mixed phases do not represent a favorable case for XSW analysis. Population of multiple atomic sites smears the adatom spatial distribution, resulting in a diminished value of a_H (and hence the observed f_H). The spatial distribution will not be well described by a single Fourier component. However, for coverages between about 0.4 and 1.0 ML, the competing surface phases are constructed of subunits having essentially the same local structure, which has been interpreted as a highly buckled dimer [15], and XSW is sensitive to short-range, not long-range, order. Thus, for coverages between 0.4 and 1.0 ML where the *local* structure appears to be unchanging, XSW can hope to determine the parameters of the local structure despite the mixed phases. One particular issue XSW can address is the composition of the buckled dimers; it is not clear from previous studies if they are Sn–Sn dimers, Sn–Si dimers, or a mixture [1,15].

For a more complete picture of the surface symmetries encountered, the reader is directed to Ref. [15]. For the purposes of the present study, we note that the (6×2) and $c(8\times4)$ phases appear to consist principally of buckled dimers, and the (5×1) phase is formed when rows (having a periodicity of $5a$) of second-layer Sn atoms form on top of the completed $c(8\times4)$ phase [15]. A schematic of the $c(8\times4)$ structure proposed in Ref. [15] is shown in Fig. 2a in plan view. Figs. 2b and 2c depict projections of a portion of the structure along the [110] and [100] directions, respectively; these projections illustrate the (004) and (022) planes used in the XSW analysis. Note that for this surface structure, there are two inequivalent Sn positions with respect to the (004) planes, and four inequivalent Sn positions with respect to the (022) planes.

4.1. $\theta < 0.75$ ML

For Sn coverages less than 0.75 ML, the XSW analyses revealed rather low values of f_{004}. This was true for surfaces exhibiting both (6×2) and $c(8\times4)$ LEED patterns. The vanishingly small value of f_{004} precluded the determination of the coherent position P_{004} from these measurements.

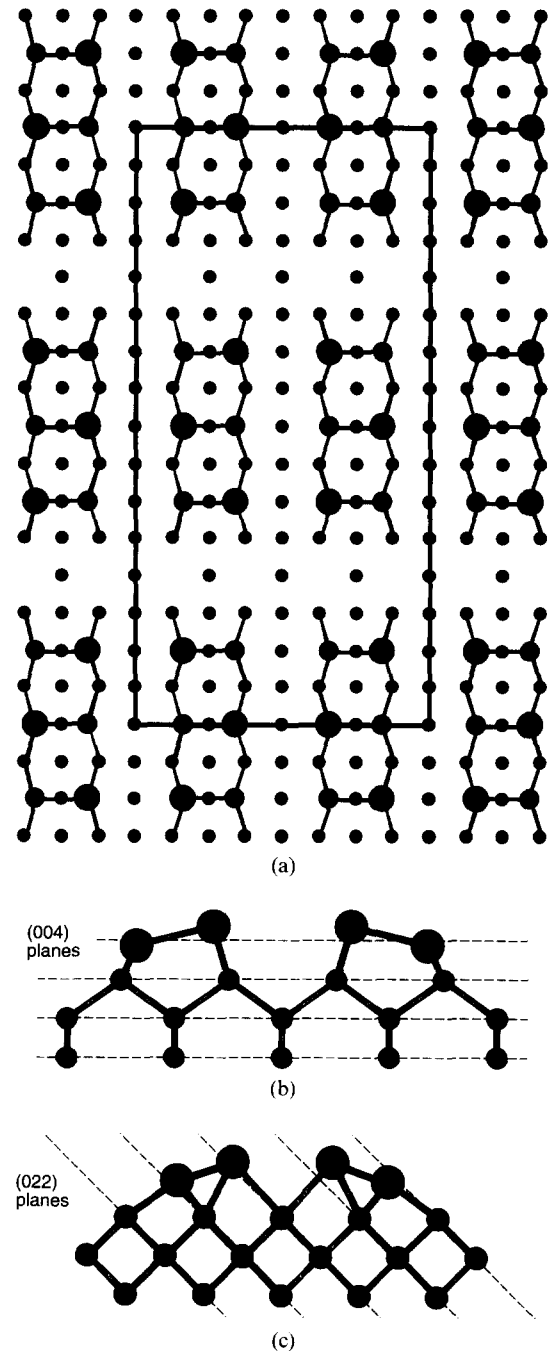

Fig. 2. Schematic diagrams of the Sn/Si(001)-$c(8\times4)$ structure depicting the arrangement of buckled Sn ad-dimers. Shaded circles are Sn atoms, and closed circles are Si atoms: (a) a plan view, with a $c(8\times4)$ unit cell outlined; (b) a [110] projection of the local structure, with (004) planes indicated; (c) a [100] projection of the local structure, with (022) planes indicated.

Fig. 3a depicts a typical result for $\theta = 0.65$ [LEED pattern was c(8 × 4)]. Ordinarily, this result would be interpreted as resulting from a disordered surface ($C \approx 0$), but this would be surprising in light of the sharp LEED patterns obtained from all preparations. Indeed, we can rule out this possibility by utilizing a different set of diffraction planes. Fig. 3b depicts an XSW analysis using the (022) reflection [21]. The substantial value of f_{022} immediately rules out the possibility of $C \approx 0$, and implicates the geometrical factor a_{004} as the cause of the low values of f_{004}.

Since these surfaces are dominated by highly buckled dimers [15], the geometrical factor is

$$a_{004} = |\cos(\pi \Delta d / d_{004})|, \quad (3)$$

where Δd is the vertical separation between the two Sn atoms in a dimer. Thus, the low value of f_{004} (coupled with the non-zero value of f_{022}) immediately renders two important pieces of information. First, there must be approximately equal numbers of "up" Sn atoms and "down" Sn atoms on the surface for all coverages investigated. Since it is unlikely that a Sn–Si dimer would fail to exhibit a preferred orientation, this constitutes strong evidence that the dimers must be composed of two Sn atoms, and that Sn–Si dimers are rare. Second, this result means that the two Sn atoms in a dimer are nearly exactly out of phase with respect to the standing wavefield [22]. For $a_{004} \approx 0^{+0.05}_{-0.00}$, we can invert Eq. (3) to give a value for Δd of 0.68 ± 0.02 Å. This can be expressed as a buckling angle of $14.0 \pm 0.5°$ by assuming a Sn–Sn dimer bond length of 2.81 ± 0.06 Å (from the covalent radius of α-Sn). For comparison, a buckling angle of 12.1° was inferred for Ge–Ge dimers on Si(001) [23,24].

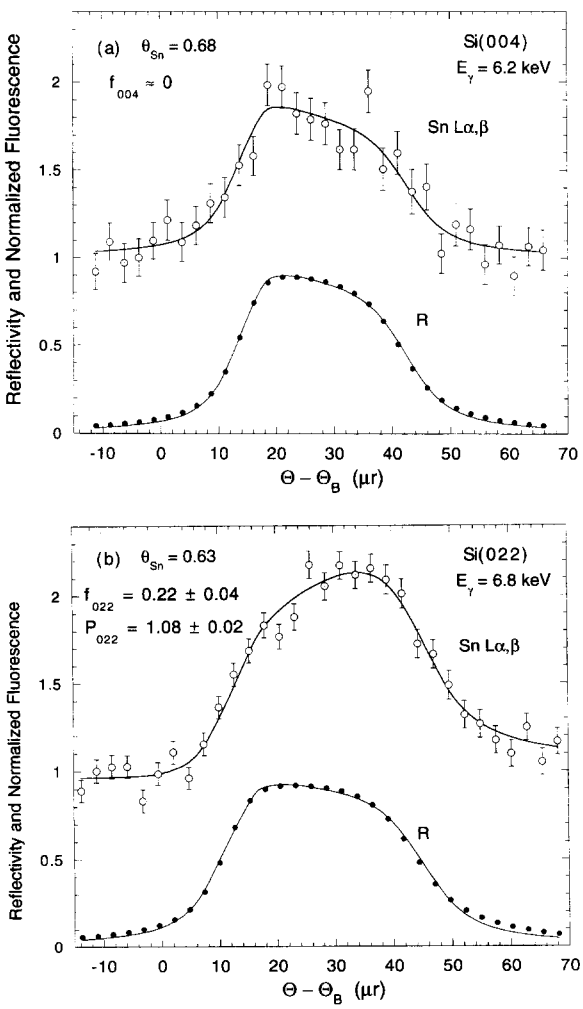

Fig. 3. XSW scan for the (a) (004) and (b) (022) diffraction planes for samples with slightly less than 0.75 ML Sn coverage.

Although the adsorption height of the dimers can not be determined in the usual way, using the value of P_{004}, it can be derived from the value of P_{022}: For an atomic spatial distribution that is centered about a two-fold symmetry site, P_{022} is equivalent to $(1 + P_{004})/2$. Thus, the measured value of P_{022} of 1.08 implies that P_{004} should equal 1.16, or, equivalently, the center of the buckled dimer is located 1.58 ± 0.04 Å above the bulk-like Si(004) surface atomic plane. This value is reasonable in light of the covalent radii of Sn (1.40 Å) and Si (1.17 Å); in the buckled dimer geometry, the adsorption height implied by P_{022} is consistent with a surface relaxation of 0.05 Å, a Sn–Sn bond length of 2.81 Å, and a mean Sn–Si bond length of 2.57 Å, equivalent to the sum of the covalent radii [25].

Even for symmetrical (unbuckled) dimers, the two Sn atoms in each dimer would occupy inequivalent positions with respect to the (022) diffraction planes. The geometrical factor f_{022} reflects both this inequivalent projection of the members of the Sn–Sn dimer along the (022) direction, and also the further inequivalence of the "up" and "down"

atoms due to dimer buckling. The complicated expression for f_{022} will be omitted here; for the dimer geometry outlined above, its value should be approximately 0.5. Even when further reduced (Eq. (2)) by the Debye–Waller factor (~ 0.9), the expected value of f_{022} for a perfectly ordered, homogeneous surface is higher than the experimental value ($f_{022}=0.22$ for $\theta=0.62$). Thus, it appears that there is a significant amount of either disorder or admixture of other phases for coverages less than 0.75 ML. This is consistent with the observations of STM [15].

4.2. $\theta > 0.75$ ML

In contrast to the lower coverage measurements, (004) XSW analyses for $\theta > 0.75$ ML exhibited substantial values of f_{004}. Fig. 4a shows the (004) results obtained for $\theta=0.78$ ML, and Fig. 4b depicts the (022) results for $\theta=0.82$ ML. Clearly, the adatom geometry has changed compared to $\theta=0.65$, yet both surfaces gave rise to sharp c(8×4) LEED patterns. If we assume the surface still consists of buckled dimers, and invert Eq. (3) for a_{004} as before, we obtain a buckling angle of $11.6\pm0.8°$ [26]. If, as discussed below, the surface is no longer uniformly covered by buckled dimers, this calculation is not valid.

Fig. 5a plots the values of the observed P_{004} and P_{022} as a function of Sn coverage, while the values of f_{004} and f_{022} are plotted in Fig. 5b. The observed LEED patterns are indicated. Note that two distinct changes occur near $\theta=0.75$ ML: the value of f_{004} increases dramatically, as discussed, and also the value of P_{022} changes suddenly. Taken together, this constitutes strong evidence for a structural change at 0.75 ML.

Interestingly, the value of f_{004} continues to rise at high Sn coverages, where the LEED pattern becomes (5×1); f_{004} becomes as high as 0.41. The STM study clearly showed that the (5×1) structure consists of second-layer Sn atoms residing on top of the initial Sn layer. Generally, occupation of two distinct atomic layers by an adatom will result in a diminished value of f_H because the different interlayer spacing of the adatom (compared to Si) will result in a projection into different sites within the bulk unit cell. The increase in f_{004} therefore

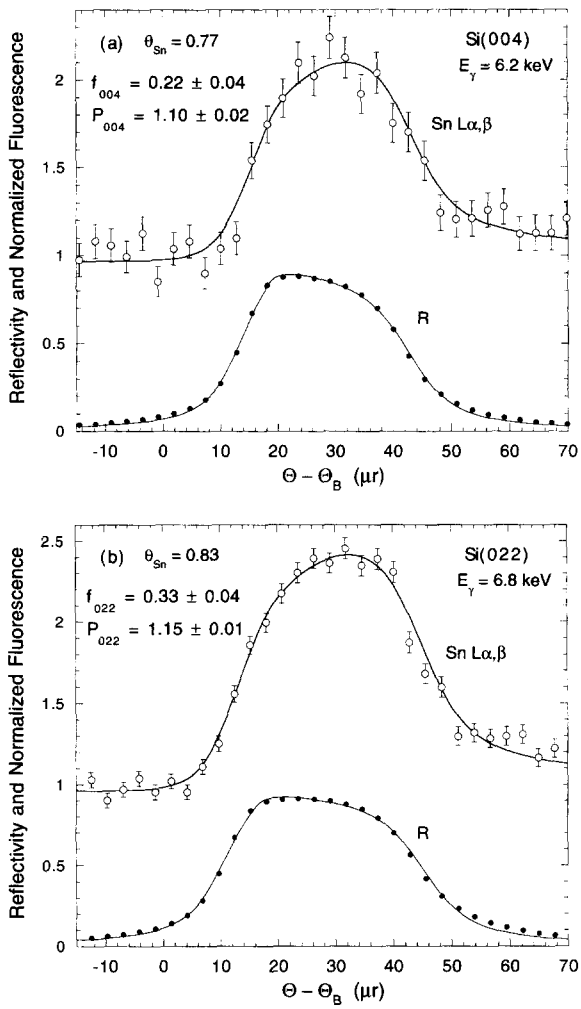

Fig. 4. XSW scan for the (a) (004) and (b) (022) diffraction planes for samples with slightly greater than 0.75 ML Sn coverage.

likely indicates that the presence of second-layer Sn atoms in the (5×1) structure unbuckles (and possibly undimerizes) the first-layer Sn atoms they cover. This would lead to a Sn spatial distribution that is more peaked than that of the c(8×4) structure, consistent with the increase in f_{004}. Furthermore, it is likely that the first-layer Sn atoms, modified by the second-layer occupancy, are chiefly responsible for the non-zero value of f_{004}. The STM study showed a large degree of inhomogeneity in the local appearance of the second-layer Sn atoms, and many dimers appear

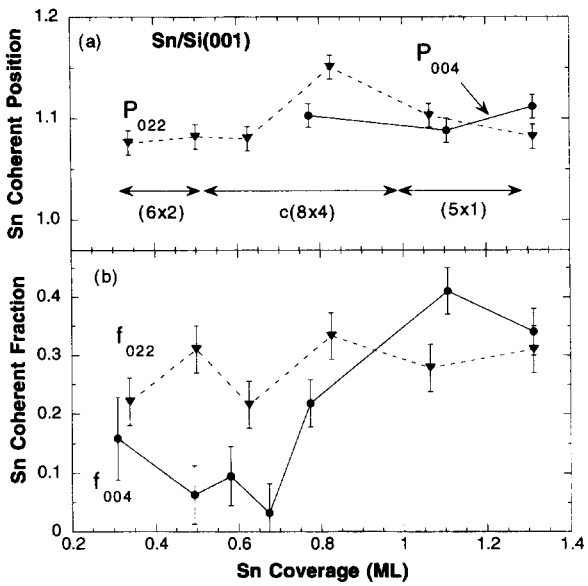

Fig. 5. The variation of the Sn (a) coherent position P_H and (b) coherent fraction f_H with Sn coverage. Note that P_{004} could not be determined for the low-coverage samples with low values of f_{004}. The LEED patterns observed are indicated schematically.

to be buckled [15]. These factors would tend to reduce the contribution to f_{004} by the second layer atoms.

As noted above, the value of P_{022} should equal that of $(1+P_{004})/2$ for an atomic spatial distribution that is centered about a twofold symmetry site. For coverages >0.75 ML, the experimental results do not obey this relationship. Thus, we conclude that the Sn atomic spatial distribution is not symmetric about the twofold site in this coverage range. For the (5×1) phase, this is not surprising, due to its complicated structure [15]. We will argue below that the c(8×4) phase in the coverage range of 0.75 to 1.0 ML should share this complication.

5. Discussion

The principal unresolved question in this study is the explanation of what causes the structural change we observe at $\theta=0.75$ ML. By all accounts, the LEED pattern (i.e., long-range order) and local symmetry (by STM) do not change at this coverage. However, an important, but generally overlooked fact is that the ideal coverage of the structural model proposed [15] for the c(8×4) phase is 0.75 ML. This same structure is thought to occur on a variety of IV/IV(001) systems up to 1 ML coverage: Pb/Si(001) [27], Pb/Ge(001) [28–30] and Sn/Si(001) [15]. To our knowledge, no previous authors have addressed where the "extra" adatoms are accommodated in these structures between 0.75 and 1.0 ML.

It is possible, of course, that the coverage scales reported earlier are simply in error by 25%: the (5×1) structure may first actually appear at 0.75 ML, neatly explaining the failure of STM to observe any "extra" Sn atoms. This hypothesis does not, however, directly explain the change in structure we observe in the middle of the coverage range of the c(8×4) phase.

Another possibility is that the earlier coverage assignments are accurate, but that the additional Sn atoms (above 0.75 ML) are accommodated in sites that are not observable by STM. The accepted structure of the c(8×4) phase is marked by one missing dimer out of every four, resulting in narrow trench-like gaps on the surface (Fig. 2). It is conceivable that the extra Sn atoms begin to populate these gaps above 0.75 ML, and thereby perturb the local structure enough to be obvious by XSW, but not by STM. However, these vacant dimer sites almost certainly exist to lessen the compressive surface stress induced by the large covalent radius of Sn compared to Si. The STM images clearly show [15] that Sn atoms in the c(8×4) phase expand into these gaps (not depicted in Fig. 2). Accommodation of additional Sn in these gaps seems unlikely to be energetically favorable; occupation of these sites that remains invisible to STM seems even less credible. Yet another possibility is that the excess Sn occupies subsurface substitutional sites, and yet does not perturb the electronic or geometrical structure sufficiently to be observable by STM. Again, this seems unlikely.

The most believable scenario is that the excess Sn occupies second-layer sites, but does not form structures that are sufficiently stable or well ordered to form LEED spots or STM features. A possible mechanism for this elusiveness could be

the high mobility that Sn would be expected to have, even at room temperature (RT). For RT deposition, Sn/Si(001) forms fairly well-ordered (metastable) structures at low coverages [15], and a sharp, (1×1) LEED pattern at $\theta\approx5$ ML [31]. Similarly, RT deposition of Sn on a Sn/Si(111)-$(\sqrt{3}\times\sqrt{3})$R30° starting template results in epitaxy of α-Sn [32]. These RT trends pervade other IV/IV(001) systems: Pb deposition on Si(001) at RT forms a rich array of coverage-dependent LEED superstructures [27], and for Pb/Ge(001), not only do superstructures form at RT, but a slow, irreversible phase transition has also been observed [28]. For present purposes, this high RT mobility may render STM imaging of the mobile, second-layer Sn atoms in excess of 0.75 ML difficult and inconsistent, as found for high coverages of Sn/Si(111) [32]. In this scenario, the mobile second-layer Sn atoms would constitute a 2D lattice gas having a weak tendency to cluster, presumably into the local arrangement found in the (5×1) phase. For a given substrate temperature, the stability of these clusters would be dictated by the density of the 2D lattice gas (i.e., the Sn coverage), as determined by classical nucleation theory [33]. Therefore, the nucleation of readily observable, stable second-layer Sn rows characteristic of the (5×1) phase would not be fomented until the second-layer sites become sufficiently populated by Sn atoms; observation of corresponding LEED features would thereby be delayed until higher coverages. We postulate this to occur at coverages close to 1 ML.

This scenario could explain our observation of a change in the XSW results at 0.75 ML that is not evident by STM or LEED. The effect of second-layer Sn atoms on the first-layer Sn geometry should be similar whether the atoms are mobile or bound in (5×1)-like rows. Specifically, we expect that the presence of a Sn dimer or row of dimers on the second layer would unbuckle (or perhaps break) the underlying Sn–Sn dimer, thereby causing the first-layer Sn atoms to attain a more uniform adsorption height. This would be manifested as an increased value of f_{004}, but would not be non-observable by STM or LEED.

Further support for this scenario can be derived from our observations of long-range order and coverage. As pointed out above, the ideal coverage of the proposed structure of the $c(8\times4)$ phase is 0.75 ML, not 1 ML. Similarly, the ideal coverage of the (5×1) phase, which has rows consisting of two Sn dimers in each $5a\times2a$ or $1a$ cell, should be 1.15–1.25 ML (0.75 ML first-layer sites + 0.4–0.5 ML second-layer sites). It has been proposed that facetting commences just above the completion of the ideal (5×1) structure [15]; the ideal (5×1) coverage calculated above is significantly lower than the value of 1.5 ML cited by Refs. [14,15] for the onset of facetting. In the present study, we observe the onset of facetting at a coverage as low as 1.32 ML. Thus, it appears that the neither the ideal (5×1) phase nor the $c(8\times4)$ phase can accommodate as much Sn as previously thought.

In summary, we find that at coverages below 0.75 ML, the Sn/Si(001) surface system is dominated by Sn–Sn dimers adsorbed 1.58 ± 0.04 Å above the bulk-like Si(004) surface atomic plane, and with a buckling angle of $14.0\pm0.5°$. A structural change is observed at $\theta=0.75$ ML that does not affect the LEED pattern. We attribute this change to a population of mobile second-layer Sn atoms that cannot be accommodated in the $c(8\times4)$ phase.

Acknowledgements

This work was supported by the US Department of Energy under contract No. W-31-109-ENG-38 to Argonne National Laboratory, contract No. DE-AC02-76CH00016 to National Synchrotron Light Source at Brookhaven National Laboratory, and by the National Science Foundation under contract No. DMR-9632593, and under contract No. DMR-9120521 to the MRC at Northwestern University.

References

[1] D.H. Rich, T. Miller, A. Samsavar, H.F. Lin and T.-C. Chiang, Phys. Rev. B 37 (1988) 10221.
[2] G. Le Lay and K. Hricovini, Phys. Rev. Lett. 65 (1990) 807.

[3] C.L. Griffiths, H.T. Anyele, C.C. Matthai, A.A. Cafolla and R.H. Williams, J. Vac. Sci. Technol. B 11 (1993) 1559.
[4] W. Dondl, G. Lütjering, W. Wegscheider, J. Wilhelm, R. Schorer and G. Abstreiter, J. Cryst. Growth 127 (1993) 440.
[5] X.W. Lin, Z. Liliental-Weber, J. Washburn, E.R. Weber, A. Sasaki, A. Wakahara and T. Hasegawa, Phys. Rev. B 52 (1995) 16 581; J. Vac. Sci. Technol. B (1995) 1805.
[6] P.R. Pukite, A. Harwit and S.S. Iyer, Appl. Phys. Lett. 54 (1989) 2142.
[7] H. Höchst, M.A. Engelhardt and I. Hernández-Calderón, Phys. Rev. B 40 (1989) 9703.
[8] W. Wegscheider, K. Eberl, U. Menczigar and G. Abstreiter, Appl. Phys. Lett. 57 (1990) 875; W. Wegscheider et al., J. Cryst. Growth 123 (1992) 75.
[9] H.-J. Gossmann, J. Appl. Phys. 68 (1990) 2791.
[10] D.W. Jenkins and J.D. Dow, Phys. Rev. B 36 (1987) 7994.
[11] T. Brudevoll, D.S. Citrin, N.E. Christensen and M. Cardona, Phys. Rev. B 48 (1993) 17 128.
[12] M. Zinke-Allmang, H.-J. Gossmann, L.C. Feldman and G.J. Fisanick, J. Vac. Sci. Technol. A 5 (1987) 2030.
[13] N. Kuwata, T. Asai, K. Kimura and M. Mannami, Surf. Sci. 143 (1984) L393.
[14] K. Ueda, K. Kinoshita and M. Mannami, Surf. Sci. 145 (1984) 261.
[15] A.A. Baski, C.F. Quate and J. Nogami, Phys. Rev. B 44 (1991) 11 167.
[16] J. Zegenhagen, Surf. Sci. Rep. 18 (1993) 199.
[17] A. Ishizaka and Y. Shiraki, J. Electrochem. Soc. 133 (1986) 666.
[18] Our AES results have a relative uncertainty from measurement to measurement of $\sim 10\%$. However, the absolute calibration of our AES scale to the actual coverage scale, making no reference to LEED superstructures, is $>20\%$. This uncertainty arises principally from uncertainties of the energy-dependent mean free path of the Auger electrons. Thus, we are unable to confirm or disprove Ueda's coverage assignments [14].
[19] B.W. Batterman and H. Cole, Rev. Mod. Phys. 36 (1964) 681.
[20] M.J. Bedzyk and G. Materlik, Phys. Rev. B 31 (1985) 4110.
[21] The [022] diffraction vector is inclined 45° from the surface normal and its projection onto the (001) plane lies 45° from the dimer rows of both domains of the two-domain surface. Thus, the two domains are equivalent with respect to this diffraction vector.
[22] This situation is closely analogous to a forbidden reflection in conventional diffraction. The phase-weighted sum of fluorescent sites vanishes (similar to a structure factor of zero).
[23] E. Fontes, J.R. Patel and F. Comin, Phys. Rev. Lett. 70 (1993) 2790.
[24] M.W. Grant, D.J. Dieleman, M.A. Boshart and L.E. Seiberling, Phys. Rev. B 49 (1994) 16 534.
[25] Note that if the subsurface Si atoms are in bulk-like positions, then the dimer buckling would imply that the "up" Sn atoms would have a substantially longer bond length to the underlying Si atoms than would the "down" Sn atoms. We expect that the subsurface Si atoms will be distorted away from bulk-like sites to minimize this disparity. Since the direction of the dimer buckling alternates along a dimer row (Fig. 2), a displacement of a Si atom towards an "up" Sn atom will also serve to move it away from a "down" Sn atom. An in-plane displacement of ~ 0.25 Å would be sufficient to bring all Sn–Si bond lengths to a value close to the sum of the covalent radii.
[26] For purposes of this calculation, we assume that $C=1$ and use a Debye–Waller factor of 0.85, consistent with previous measurements of dimerized adatoms on the Si(001) surface. For details, see Y. Qian, P.F. Lyman and M.J. Bedzyk, Scanning Microsc. 9 (1995) 969.
[27] R.G. Zhao, J.F. Jia and W.S. Yang, Surf. Sci. 274 (1992) L519.
[28] Y. Zhang, R.G. Zhao and W.S. Wang, Surf. Sci. 293 (1993) L821.
[29] L. Seehofer, G. Falkenberg, R. Rettig and R.L. Johnson, J. Phys. (Paris) IV 4 (1994) C9–97.
[30] W.S. Yang, X.-D. Wang, K. Cho, J. Kishimoto, T. Hashizume and T. Sakurai, Surf. Sci. 310 (1994) L625; Phys. Rev. B 51 (1995) 7571.
[31] I. Andriamanantenasoa, J.P. Lacharme and C.A. Sébenne, Surf. Sci. 189/190 (1987) 563.
[32] D.T. Wang, N. Esser, M. Cardona and J. Zegenhagen, Surf. Sci. 343 (1995) 31.
[33] D. Walton, J. Chem. Phys. 37 (1962) 2182.